

University of Mississippi

eGrove

Faculty and Student Publications

Physics and Astronomy

9-1-2022

India's First Robotic Eye for Time-domain Astrophysics: The GROWTH-India Telescope

Harsh Kumar

Indian Institute of Technology Bombay

Varun Bhalerao

Indian Institute of Technology Bombay

G. C. Anupama

Indian Institute of Astrophysics

Sudhanshu Barway

Indian Institute of Astrophysics

Judhajeet Basu

Indian Institute of Astrophysics

See next page for additional authors

Follow this and additional works at: https://egrove.olemiss.edu/physics_facpubs



Part of the [Astrophysics and Astronomy Commons](#)

Recommended Citation

Kumar, H., Bhalerao, V., Anupama, G. C., Barway, S., Basu, J., Deshmukh, K., De, K., Dutta, A., Fremling, C., Iyer, H., Jassani, A., Joharle, S., Karambelkar, V., Khandagale, M., Krishna, K. A., Kulkarni, S., Mate, S., Patil, A., Phanindra, D., ... Stanzin, U. (2022). India's first robotic eye for time-domain astrophysics: The growth-india telescope. *The Astronomical Journal*, 164(3), 90. <https://doi.org/10.3847/1538-3881/ac7bea>

This Article is brought to you for free and open access by the Physics and Astronomy at eGrove. It has been accepted for inclusion in Faculty and Student Publications by an authorized administrator of eGrove. For more information, please contact egrove@olemiss.edu.

Authors

Harsh Kumar, Varun Bhalerao, G. C. Anupama, Sudhanshu Barway, Judhajeet Basu, Kunal Deshmukh, Kishalay De, Anirban Dutta, Christoffer Fremling, Hrishikesh Iyer, Adeem Jassani, Simran Joharle, Viraj Karambelkar, Maitreya Khandagale, K. Adithya Krishna, Sumeet Kulkarni, Sujay Mate, Atharva Patil, and D. V. S. Phanindra



India's First Robotic Eye for Time-domain Astrophysics: The GROWTH-India Telescope

Harsh Kumar¹ , Varun Bhalerao¹ , G. C. Anupama² , Sudhanshu Barway² , Judhajeet Basu² , Kunal Deshmukh^{3,4} , Kishalay De^{5,6} , Anirban Dutta^{2,7} , Christoffer Fremling⁵ , Hrishikesh Iyer⁸ , Adeem Jassani¹ , Simran Joharle^{9,10} , Viraj Karambelkar^{1,5} , Maitreya Khandagale¹, K Adithya Krishna¹, Sumeet Kulkarni¹¹ , Sujay Mate¹² , Atharva Patil¹³, DVS Phanindra² , Subham Samantaray¹ , Kritti Sharma¹⁴ , Yashvi Sharma^{1,5} , Vedant Shenoy¹, Avinash Singh^{2,15} , Shubham Srivastava¹⁶ , Vishwajeet Swain¹ , Gaurav Waratkar¹ , Dorje Angchuk¹⁷, Padma Dorjay¹⁷ , Tsewang Dorjai¹⁷, Tsewang Gyalson¹⁷, Sonam Jorphail¹⁷, Tashi Thsering Mahay¹⁷, Rigzin Norbu¹⁷, Tarun Kumar Sharma¹⁸ , Jigmet Stanzin¹⁷, Tsewang Stanzin¹⁷ , and Urgain Stanzin¹⁷

¹ Department of Physics, Indian Institute of Technology Bombay, Powai, 400 076, India; harshkosli13@gmail.com

² Indian Institute of Astrophysics, 2nd Block 100 Feet Rd, Koramangala Bangalore, 560 034, India

³ Department of Metallurgical Engineering and Materials Science, Indian Institute of Technology Bombay, Powai, Mumbai-400076, India

⁴ Department of Physics and Astronomy, Texas Tech University, PO Box 41051, Lubbock, TX 79409, USA

⁵ Division of Physics, Mathematics and Astronomy, California Institute of Technology, Pasadena, CA 91125, USA

⁶ MIT-Kavli Institute for Astrophysics and Space Research, 77 Massachusetts Ave., Cambridge, MA 02139, USA

⁷ Pondicherry University, R.V. Nagar, Kalapet, 605014, Puducherry, India

⁸ Department of Electrical and Computer Engineering, University of Illinois at Urbana-Champaign, Urbana, IL 61801, USA

⁹ Fergusson College, Shivajinagar, Pune, Maharashtra, 411 004, India

¹⁰ Heidelberg University, Grabengasse 1, D-691 17, Heidelberg, Germany

¹¹ 204 Lewis Hall, The University of Mississippi, Oxford, MS 38677, USA

¹² Department of Astronomy and Astrophysics, Tata Institute of Fundamental Research, Mumbai, 400005, India

¹³ Graduate Institute of Astronomy, National Central University, 32001, Taiwan

¹⁴ Department of Mechanical Engineering, Indian Institute of Technology Bombay, Powai, Mumbai-400076, India

¹⁵ Hiroshima Astrophysical Science Center, Hiroshima University, Higashi-Hiroshima, Hiroshima, 739-8526, Japan

¹⁶ Astrophysics Research Centre, School of Mathematics and Physics, Queen's University Belfast, Belfast, BT7 1NN, UK

¹⁷ Indian Astronomical Observatory, Indian Institute of Astrophysics, Post Box No. 100, Leh-Ladakh (UT) 194 101 India

¹⁸ Physikalisches Institut der Universität zu Köln, Zùlpicher Strasse 77, D-50937 Cologne, Germany

Received 2022 May 13; revised 2022 June 22; accepted 2022 June 22; published 2022 August 10

Abstract

We present the design and performance of the GROWTH-India telescope, a 0.7 m robotic telescope dedicated to time-domain astronomy. The telescope is equipped with a 4k back-illuminated camera that gives a $0^{\circ}.82$ field of view and a sensitivity of $m_g \sim 20.5$ in 5 minute exposures. Custom software handles observatory operations: attaining high on-sky observing efficiencies ($\gtrsim 80\%$) and allowing rapid response to targets of opportunity. The data processing pipelines are capable of performing point-spread function photometry as well as image subtraction for transient searches. We also present an overview of the GROWTH-India telescope's contributions to the studies of gamma-ray bursts, the electromagnetic counterparts to gravitational wave sources, supernovae, novae, and solar system objects.

Unified Astronomy Thesaurus concepts: [Astronomical instrumentation \(799\)](#); [Astronomical detectors \(84\)](#); [Automated telescopes \(121\)](#); [CCD photometry \(208\)](#); [Optical observatories \(1170\)](#); [Optical astronomy \(1776\)](#); [Time domain astronomy \(2109\)](#)

1. Introduction

Time-domain astrophysics (TDA) has become a major thrust area around the world and is poised to continue growing in the coming decade (Srinivasan et al. 2004; de Zeeuw & Molster 2007; NRC Decadal Survey 2010; National Academies of Sciences, Engineering, & Medicine 2021). The studies of transient sources allow us to probe some of the most extreme environments in the universe and, in turn, address open questions from such diverse fields as the distributions of planets around other stars, the fates of massive stars, the nature of accretion and jets, and nucleosynthesis in the universe (see for instance LSST Science Collaboration et al. 2009; Kasliwal 2011, and references therein). Time-domain studies span many orders of magnitudes in timescales. In optical bands, new high-speed

instruments study variability at subsecond timescales (Dhillon et al. 2007, 2016, etc.), while long-term variability studies have spanned decades (Grindlay et al. 2009; Graham et al. 2015).

The varied classes of targets studied in TDA each have their specific requirements from observational facilities. Many sources like supernovae, novae, period objects like binaries, etc., require monitoring at a cadence of one or a few days: a task that is cumbersome for classically scheduled telescopes but straightforward for queue-scheduled ones. Fast transients like afterglows of gamma-ray bursts (GRBs) or electromagnetic counterparts to gravitational wave (EMGW) sources demand fast responses within minutes or even seconds of discovery of the transient. They also require a geographically distributed network of observatories to ensure that the target is visible to at least some of them. Some sources require continuous monitoring, unhindered by the diurnal cycle. This too requires a geographically spread out set of observatories coordinating their efforts. To address these issues, various global networks have been created with telescopes geographically distributed



Original content from this work may be used under the terms of the [Creative Commons Attribution 4.0 licence](#). Any further distribution of this work must maintain attribution to the author(s) and the title of the work, journal citation and DOI.

around the world—for instance, the Global Relay of Observatories Watching Transients Happen (GROWTH; Kasliwal et al. 2019), Las Cumbres Observatory Global Telescope (LCOGT; Brown et al. 2013), Global Rapid Advanced Network Devoted to the Multi-messenger Addicts (GRANDMA; Antier et al. 2020), and MASTER (Lipunov et al. 2010). Typically, such networks have had more telescopes in the “western hemisphere,” with limited participation from “eastern” countries. Indian astronomers have been active in time-domain astrophysics using a variety of optical and infrared facilities in the country (for a brief overview of the facilities, see Sagar 2017 and references therein). However, these facilities are classically scheduled and heavily subscribed, with time-domain observations largely executed through a limited number of target-of-opportunity (ToO) triggers.

This motivated us to set up the GROWTH-India Telescope (GIT), a fully autonomous dedicated telescope for time-domain astrophysics. The facility was set up with certain key goals in mind. The main focus was to have a fully automated system that can respond to fast transient triggers with minimal lag, including autonomous responses to GCN (Barthelmy et al. 2000) and similar triggers. A closely aligned goal was to create automated and standardized pipelines for all data processing so that the team can focus on interpretation rather than data reduction. The telescope needed to be sensitive to about 21 mag in optical, with $\sim 1^\circ$ field of view. We opted for an off-shelf telescope and camera for rapid deployment, high reliability, and ready availability of technical support. GIT would work closely with partners in the GROWTH sharing the key science goals (Section 6).

In this paper, we describe the configuration, performance, and some scientific results from GIT. The paper is organized as follows. In Section 2 we describe the site, telescope, and instruments. Section 3 deals with the nightly autonomous observing procedures, while the data processing is described in Section 4. The sensitivity and performance of the telescope are discussed in Section 5. Lastly, Section 6 enumerates the key science goals of GIT and presents some results from the first few years of operation.

2. System Configuration

GIT is a 70 cm telescope designed for autonomous operations, backed up by local and remote observing capabilities. The primary camera is an Andor iKon-XL 230 CCD camera with a 16.8-megapixel back-illuminated sensor. The telescope and camera have been chosen to provide a unique combination of a 0.7° wide field of view (FoV) and good sensitivity. The telescope was installed and commissioned in the summer of 2018 and is jointly operated by the Indian Institute of Astrophysics and the Indian Institute of Technology Bombay.

2.1. Observing Site Location

GIT is situated at the Indian Astronomical Observatory (IAO), located atop Mt. Saraswati, Digpa Ratsa Ri in Hanle, Ladakh. The observatory is located at latitude $32^\circ 46' 46''$ N and longitude $78^\circ 57' 51''$ E, at an altitude of ~ 4500 m above sea level. The IAO site has ~ 190 clear photometric nights per year (Cowsik et al. 2002). IAO has meager precipitation of < 7 mm annually, thanks to Himalayan mountains that cast a rain shadow on the observatory. With low temperature, low

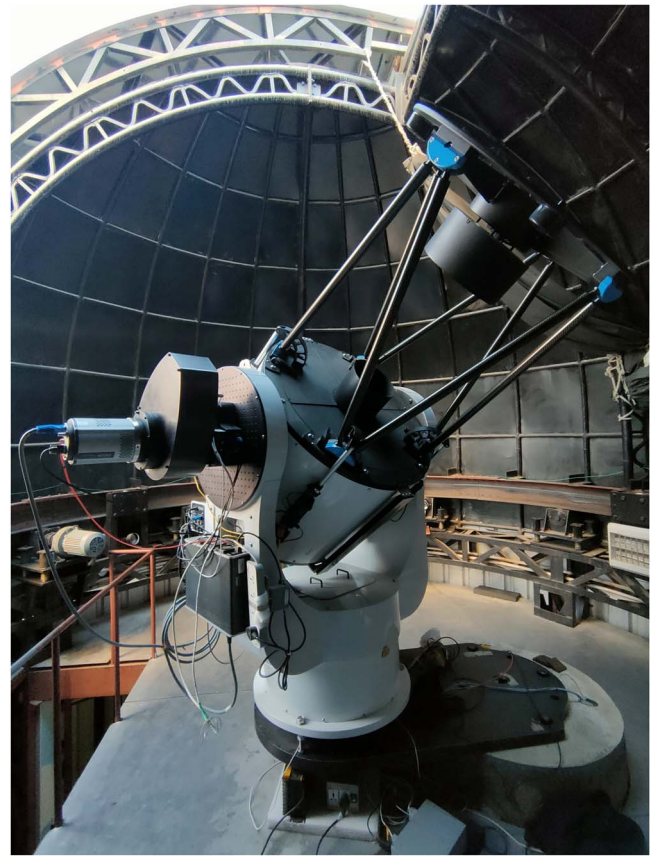


Figure 1. GROWTH-India Telescope inside the enclosure. The Andor camera is shown mounted on the telescope.

humidity, a typical seeing of $< 1''$ (Cowsik et al. 2002), and median sky brightness of $\mu_V = 21.28$ mag/arcsec² (Stalin et al. 2008), IAO is one of the best sites for optical astronomy in India. The observatory has its weather station accessible by all telescopes present at the observatory. However, in the interest of an additional level of safety, the weather station is not directly integrated into the telescope system, and the dome closure/opening is handled by the staff at other telescopes of the observatory. The observatory has an engineering team that regularly handles the maintenance of the telescope system. The observatory is remotely accessible through a satellite link from the CREST campus of the Indian Institute of Astrophysics, Bangalore.

2.2. Telescope

The telescope is a Planewave 0.7 m diameter primary mirror telescope with a Corrected Dall-Kirkham (CDK) optical design¹⁹ (Figure 1). With a focal ratio of $f/6.5$ and focal length of 4540 mm, the telescope provides a 70 mm image circle, corresponding to a $\sim 0^\circ.86$ diameter circle on the sky. The Nasmyth focus design and dual truss structure make it possible to mount two instruments simultaneously and switch between them with minimal overheads. This CDK telescope is driven by integrated direct-drive motors, providing zero backlashes, zero periodic error, and requires minimal maintenance. The telescope can reach slewing speed of up to 50 degrees s⁻¹ enabling it to track fast-moving satellites and near-

¹⁹ <https://planewave.com/product/cdk700-0-7m-cdk-telescope-system/>

Earth objects. Further, the telescope has a very good pointing accuracy of $10''$ and tracking accuracy of $<1''$ for a typical 300 s exposure. For all practical purposes, we limit the longest exposure to 10 minutes. The full specifications of the telescope are listed in Table 1.

2.3. Instruments

GIT uses an Andor XL 230-84 CCD as its primary instrument. In addition, the system's performance has been tested with APOGEE Alta U32 and SBIG STF-8300EN instruments which were used on the system during the commissioning phase and during the unavailability of the primary camera due to technical failures. Section 2.3.1 provides details of all cameras utilized on GIT to date. The cameras are operated through automated command-line scripts to perform all operations.

2.3.1. Primary Instrument: Andor

The primary instrument for GIT is an Andor XL 230 camera, which is also in use at present. This 4096×4108 pixels camera, in combination with the CDK-700 telescope, provides an effective field of view of $49'$ radius circle. This back-illuminated camera has high quantum efficiency (QE) of $>95\%$. The built-in thermoelectric (TE) system and air cooling can lower the operating temperatures to 60° below ambient. The operating temperatures can be lowered further with water cooling, but this is not used at GIT due to low ambient winter temperatures and robustness requirements for an autonomous telescope. We chose the CCD with a $15 \mu\text{m}$ pixel size to sample the point-spread function (PSF) properly, providing a pixel scale of $0.676''$. The CCD has a full well depth of $1,50,000 e^-$, providing a large dynamic range. With linearity of $>99\%$ and a very low dark current (~ 0.0024 ADUs/pix/s), the CCD is well suited to long exposures without significant nonuniformity in images. The CCD supports a wide range of readout speeds, from a 10 kHz readout giving a noise of just $3.5 e^-$ to a fast 4 MHz mode that allows a full-frame readout in just 4 s, at the cost of a higher $23.4 e^-$ readout noise. In practice, we typically use a single-port readout at 2 MHz. User-definable binning makes the CCD versatile to use in desired science cases. Detailed specifications of this Andor camera are listed in Table 1, while more details from the vendor are available.²⁰

2.3.2. Apogee

An Apogee Alta U32 camera with a 3-megapixel Kodak Blue Plus sensor was used at GIT from 2020 August–2021 March. The camera has a rectangular image layout with 2184×1472 pixels, where each square pixel has a 6.8 micron size ($0''.346$ on the sky). The camera has an imaging area of 14.8×10.0 mm that provides an FoV of $11'.17 \times 7'.52$. The camera's full well capacity is $55,000 e^-$ a peak QE (610 nm) $\sim 85\%$. The camera features TE cooling with forced air, which enables it to cool to a maximum of 50°C below ambient temperature with a temperature stability of $\pm 0.1^\circ\text{C}$. This camera can expose in the range of 30 ms to 183 minutes with 2.56 microsecond increments. The system is read out at 1 MHz with a low readout noise of $8 e^-$.

²⁰ <https://andor.oxinst.com/products/ikon-xl-and-ikon-large-ccd-series/ikon-xl-230>

Table 1
Planewave CDK-700 Telescope and Andor iKon-XL 230 Camera Specifications

Telescope Specifications	
Optical Design	Corrected Dall-Kirkham (CDK)
Mount type	Alt-Az mount
Aperture	700 mm (27.56 inch)
Focal Length	4540 mm
Focal ratio	6.5
Central Obstruction	47% of Mirror Diameter
Optical Tube	Dual truss structure with Nasmyth focus
Back focus	309 mm from Mounting Surface
Optical Performance	1.8 micron rms spots
Field of View	70 mm image circle ($0^\circ 86'$)
Pointing Accuracy	$10''$ rms
Maximum Altitude for pointing	88° creating a zenith blind spot of 6.5 deg^2
Pointing Precision	$2''$
Tracking Accuracy	$<1''$ error over 10 minute period
Field De-Rotator Accuracy	3 microns of peak to peak error at 35 mm off-axis over 1 hour of tracking
Primary Optical Diameter	700 mm (27.56 inch)
Secondary Optical Diameter	312.4 mm
Tertiary Optical Major Diameter	152.4 mm
Mirror Material (All)	Fused silica (quartz)
Camera Specifications	
Sensor Type	CCD230XL-84 midband AR coating
Pixels	$4096 \text{ (H)} \times 4108 \text{ (V)}$
Pixel size	$15 \times 15 \mu\text{m}$
Pixel scale	$0''.676 \text{ pix}^{-1}$
Image area	$61.4 \text{ mm} \times 61.4 \text{ mm}$
System Window transmission	$>98\%$
Cooling	-55°C air TE cooled, up to -100°C deep TE cooled. Operated at -40°C
Well depth	$1,50,000 e^-$
Readout rates	0.1, 1, 2, 4 MHz
Readout noise	3.8, 8.5, 12.0, $23.0 e^-$
Dark current @ -55°	$0.001 e^-/\text{pixel/s}$
Peak quantum efficiency	$>95\%$
Linearity	$>99\%$
Timestamp	IRIG-B GPS with 10 ms resolution
Gain	$1 \times 1.04 e^-/\text{ADU}$
Depth (300 s exposure r'-band)	$\sim 20.5 \text{ mag}$

Note. Default values are indicated by bold text.

2.3.3. SBIG STF-8300EN

Another camera used at GIT is an SBIG STF-8300EN camera with a Kodak KAF-8300 CCD sensor with a 3326×2504 pixel array. Each pixel is $5.4 \mu\text{m}$ square in size, providing a plate scale of $0''.24$. Its 8.3 million pixels camera

gives an imaging area of $17.96 \text{ mm} \times 13.52 \text{ mm}$. The camera has a high readout speed, enabling it to read the entire frame in $\sim 1 \text{ s}$ with a typical readout noise of $9.3 e^-$. The even illuminated shutter helps in taking exposures as short as 0.1 s . On the higher end, an hour-long exposure can be obtained. This SBIG camera has a higher dark current of $0.15 e^-/\text{pix}/\text{s}$ despite an ability to cool up to $40\text{--}45^\circ\text{C}$ below ambient temperature. Compared to our other two cameras, this camera has a lower full well capacity ($25,000 e^-$) and QE (56%).

2.4. Filter System

SDSS u' g' r' i' z' filters (Figure 2) are integrated into a filter wheel assembly design. The closed-loop control system of the filter wheel provides precise position and velocity control. The system is realized with a PSoC5LP microcontroller unit (MCU) based on system-on-chip (SoC) architecture. The filters are arranged in a wheel that can rotate in both clockwise and anticlockwise directions to minimize the filter change time while changing extreme position filters. A python-based script communicates with the filter wheel via an RS232 interface to perform all operations like the status of the wheel, homing position, current filter position, filter change operations, etc. The typical filter change time among adjacent filters is 2.30 s .

3. Observing With GIT

GIT operates in a default automated mode for nightly observations. The entire telescope assembly operations are controlled by two PCs that run on the Linux and Windows operating systems. The core component is the Linux PC, which runs the custom python-based operations software for GIT. This includes scheduling, controlling the camera, filter wheel, data storage and archiving, listening for target-of-opportunity commands, error reporting, etc. The telescope and dome are controlled by the Windows PC that hosts the software for the telescope and dome controls. This software opens a socket to send and receive commands for various operations of the telescope and dome, thus controlling them via communicating over Ethernet without any manual intervention. For higher-level operations like rebuilding the pointing model, the observer directly accesses the software through the Windows PC at the telescope site. We discuss key components of the control software in the following sections.

3.1. Observation Scheduling

The default robotic observation mode of GIT is the queue-based observation mode. Observation scheduling of GIT is illustrated in Figure 3. An object list is prepared before starting the nightly observations, containing all relevant information for selected targets. This list is parsed to the scheduling computer, which orders the targets based on their priority assigned by the observer. The observer chooses this priority by taking a particular target's set time and scientific importance into account. The control computer automatically takes the information from the object list for any particular object and performs observations. New targets like gamma-ray bursts (GRBs) can be manually or automatically added to the queue at any time by using specialized remote scripts. This is particularly important for rapid response to GRBs etc. Once a target is added to the queue, it is processed as per the assigned priority like any other target in the queue. This means that the ongoing image sequence is finished before switching to any such new target.

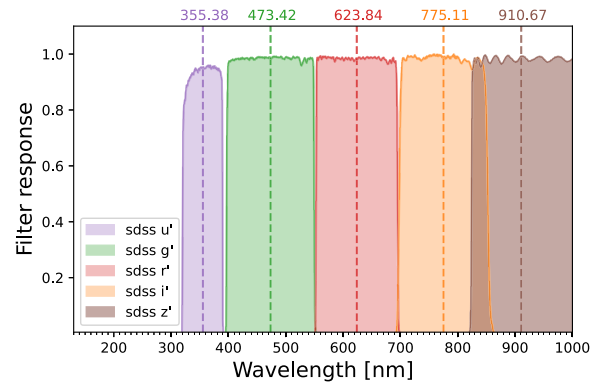


Figure 2. Filter response curves for SDSS prime filter set used at GIT. The effective wavelengths for each filter are shown by vertical dashed lines and their values are quoted at the top of the plot.

3.2. Calibration Image Acquisition

Nightly observations begin with a series of calibration exposures that are used for processing all science images acquired during that night.

3.2.1. Bias Frames

Bias frames are zero-second readouts to measure the unwanted electronic signal. Bias frames for our primary Andor camera are stable throughout the night. Therefore, we acquire these frames at the start and end of the night. The CCD is cooled to -40°C , which helps stabilize the bias frames despite ambient temperature fluctuations.

3.2.2. Dark Frames

A dark frame measures the thermal noise of the camera, which is acquired by taking images with the shutter closed to avoid external photons contributing to the image counts. We minimize the dark current by cooling the camera to -40°C . As mentioned in Section 2.3.1, the Andor CCD has a very low dark current. To verify the same, we acquired the dark frames at a fixed temperature at various exposure times ranging from $150\text{--}700 \text{ s}$ in steps of $50\text{--}100 \text{ s}$. Using a linear fit to the data, we obtained a typical dark current of $0.0052 \text{ ADUs}/\text{pix}/\text{s}$ at -40°C CCD temperature, broadly consistent with the camera datasheet. This amount of dark current does not impact the science exposure. Hence, the dark frame acquisition can be omitted for exposure $< 600 \text{ s}$.

3.2.3. Flat Frames

Twilight flat frames are used in GIT to correct the pixel response of CCD. A python-based code automatically acquires well-exposed flat frames for all filters during the evening twilight. u' and z' band flats are acquired first as they require brighter sky conditions due to high extinction in these bands. These are followed by g' , r' , and i' band exposures. The code checks the count levels in the images and eliminates any saturated or underexposed flat images. It adjusts the exposure time for subsequent flat frames to maintain median counts in the range of $30,000\text{--}450,000$.

3.3. Nonsidereal Mode Observations

Nonsidereal observing has been integrated with the main scheduler of GIT to streamline observations of moving objects.

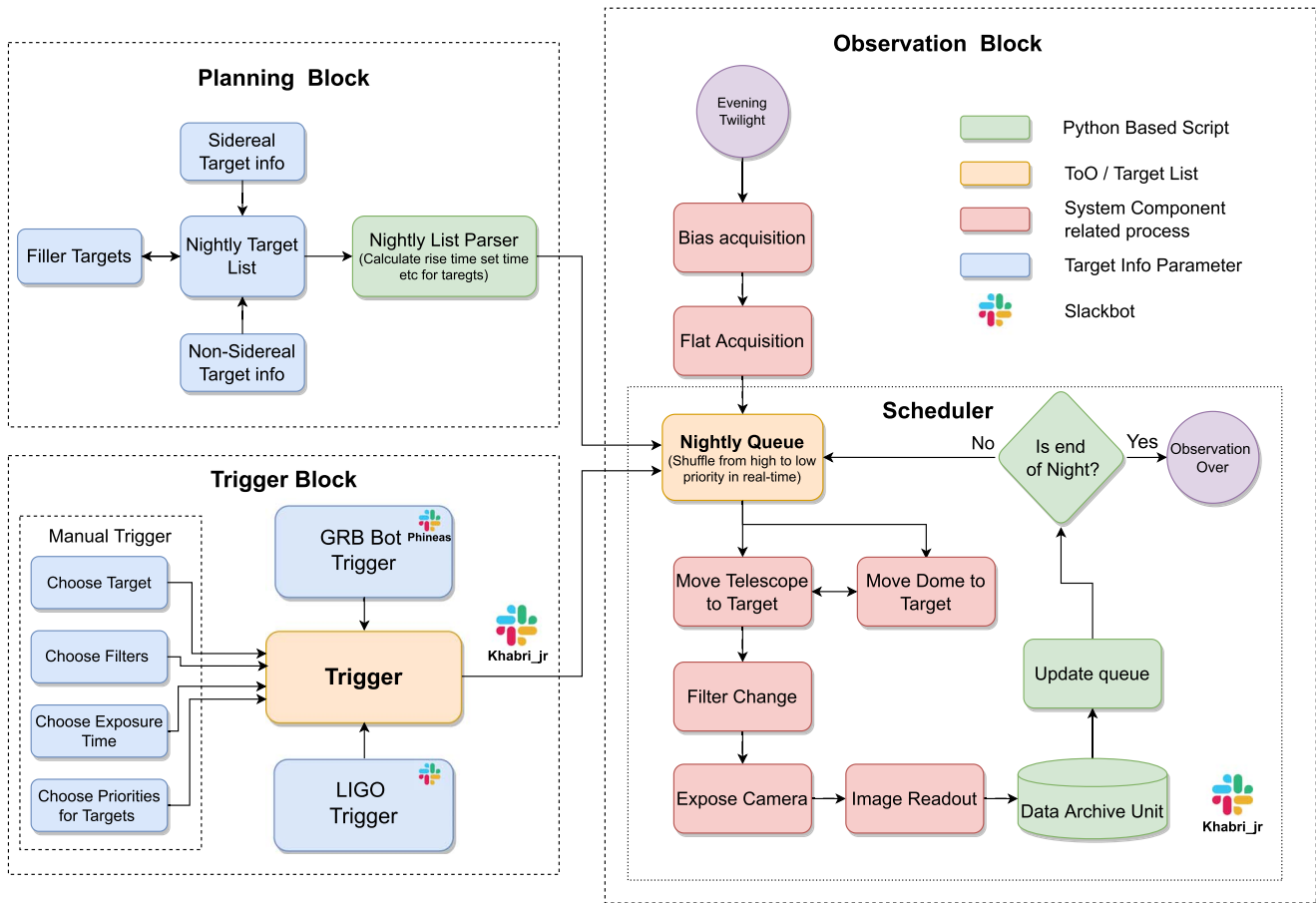


Figure 3. Observation procedure of GIT. The procedure is broadly divided into three blocks: “Planning” of targets (top left block), “Observations” which includes scheduling (right block), and adding additional targets using “Triggers” (lower left block). Observations are automated and are monitored by Slack bots.

With GIT, we perform two types of objects in nonsidereal mode: (1) confirmation of newly discovered near-Earth objects (NEOs) by GROWTH partners and other observers, and (2) follow-up observations of specific targets with confirmed orbits.

Due to the significant sky plane motion of these objects with respect to fixed background stars, the coordinates of these targets keep on changing with time. For objects confirmed by Minor Planet Center (MPC), a list of targets is prepared as per scientific interests. This list resides at IIT Bombay and comprises designations and tentative observation times of the objects. Daily at 5 PM local time, the coordinates of these nonsidereal targets are updated automatically by querying the MPC database. After querying the coordinates, a nonsidereal nightly file is generated as per the required format of the GIT scheduler, which is then synced automatically to the system at the observatory in Hanle, where it gets combined with the sidereal target list. Since the nonsidereal targets may have a significant sky plane motion, we approximate the coordinates of the targets at the time of observation by linearly extrapolating the coordinates in the nightly file. For a potential near-Earth object (NEO) discovered on the same night, the nonsidereal observations can be triggered on GIT in real time, thus enabling active follow-up of these candidates.

3.4. Helper Bots

The GIT system is integrated with several helper “bots” that monitor various operational parameters. These bots perform various tasks like automatically triggering telescopes for ToO

observations, monitoring observation as well as data processing, and summarizing the last night’s observations in the form of a nightly report. These reports are then posted on Slack²¹ groups for human inspection. In critical situations, telephonic / text message alerts can also be sent to designated users.

“Khabri_Jr”: GIT observations are monitored by the Khabri_Jr Slack bot. This bot updates the observers about a night’s observation plan and sends near real-time telescope observation updates via Slack. In case of instrument failures, the scheduling system can debug first-order errors. However, in certain cases, when the debugger fails to solve the problem, the Slack bot can identify the errors in the real-time observation log and notify designated users by a telephone call through a “Twilio” API²² so that debugging can be handled manually.

“Phineas”: This Slack bot continuously looks for the GRB alerts on the Gamma-ray Coordinates Network/Transient Astronomy Network (GCN/TAN) server.²³ Upon receiving a trigger alert, the bot checks it against triggering criteria for GIT and generates a trigger if these criteria are met. The bot sends the generated trigger to the telescope scheduling computer to add it to the main queue. A similar bot looks for gravitational wave (GW) event candidates during the observing run of the advanced GW detectors (LIGO, Virgo, Kagra) and notifies designated users through a phone call. For future runs, this

²¹ <https://slack.com/intl/en-in/>

²² <https://www.twilio.com/voice>

²³ <https://gcn.gsfc.nasa.gov/about.html>

script is also being upgraded to create an observing schedule and start observations in parallel to the user notifications.

“Khabri”: The GIT automated data reduction pipeline is integrated with Khabri (messenger) bot, which tracks data download and reduction processes. Near real-time processing, updates are sent to Slack during data processing. On completion of data reduction, the bot generates a summary report which contains information about the observed targets, time of observations, filter information, reduction status, and GIT observation performance statistics for last night’s observations. At the end of each night’s observation, the bot generates nightly statistics plots for images’ seeing and depth variation during the night as a part of the summary report.

“Gitty”: This bot is designed to send data to relevant observers automatically. After the generation of the nightly summary report, the bot filters out data under different proposals and syncs the processed data to the necessary destinations for observers to access in minimal time.

4. Data Processing

The automated scripts regularly download data from the observatory without any human intervention. Once downloaded, this data is processed by a fully automated data reduction pipeline and archived.

4.1. Data Transfer

All the raw data are stored at the data storage unit at IAO and need to be transferred to IIT Bombay for processing. These data transfers are executed through the CREST campus of IIA, which is connected to IAO through a satellite link. Data are downloaded to the data relay unit at CREST in the daytime for regular observations. However, we download data in real time via automated download scripts for important time-constrained observation. Network-attached storage (NAS) at the CREST also serves as a redundant backup of all raw data. The typical GIT raw data load for a single night is ~ 3 Gigabytes. Data files arrive at CREST and are immediately copied to IIT Bombay over the internet for further processing. A NAS system at IIT Bombay archives the raw as well as the processed data that can be accessed by an internal query interface. All the data remain proprietary.

4.2. Image Reduction

The image reduction and processing pipeline handles all tasks required for converting the observations into values ready for interpretation.

4.2.1. Preprocessing

To obtain the flux from an astronomical source, all raw GIT exposures taken with a CCD imager have to go through a set of generic steps before further image-specific processing. These include bias subtraction, flat-fielding using the bias and flat frames obtained on the same night, and cosmic-ray correction using *Astro-SCRAPPY* (McCully & Tewes 2019) package. The final preprocessing step is to calculate the astrometric solution to map pixel coordinates to sky coordinates, using the *solve-field* offline package of *astrometry.net* (Lang et al. 2010).

4.2.2. Photometry

Upon preprocessing, the images are processed via standard image processing routines. All point sources are extracted using the *SExtractor* (Bertin & Arnouts 1996). These sources are cross-matched with Pan-STARRS DR1 (Chambers et al. 2016) catalog through a *VizieR* query to obtain the zero-points of the image. The brightness of sources is estimated using PSF photometry on the source of interest. To perform PSF photometry, we obtain the PSF profile of the sources in the image using the *PSFEX* package (Bertin 2011) and convolve it with the source image to estimate the source flux. The instrumental magnitude thus obtained is corrected using an earlier estimated zero-point to obtain the standard magnitude of the source.

4.2.3. Image Subtraction

In some instances, the source of interest lies embedded inside their host galaxies, which makes it difficult to perform accurate photometry on these objects due to host contamination. Broadly, searching for new transients in the image also requires image subtraction. Such specific images of interest (identified by a header flag) go through another set of data reduction steps in the form of image subtraction and candidate search.

Image subtraction is a numeric method to subtract a deeper reference image from the science image of interest. The GIT Image subtraction pipeline is based on the ZOGY algorithm (Zackay et al. 2016). Owing to the relatively large FoV, we first divide the processed image into smaller cutouts to reduce the impact of PSF and background variation across the image. Corresponding Pan-STARRS DR1 (PS1) image cutouts are downloaded as reference images using *panstamps*.²⁴ Astrometric uncertainties in science and reference images are reduced by a cross match of positions with Gaia Data Release 2 (Brown et al. 2018 Gaia DR2) catalog. *SWarp* (Bertin et al. 2002) is used to resample both science and reference images on the same astrometric grid to align their position angles. The reference image is scaled in flux to the science image flux level based on the local ratio of pixel scales and the zero-point of images. Finally, the resampled flux-matched science and reference images, the PSF model, the rms images, and the astrometric uncertainties are used as input to *pyzogy* (Guevel & Hosseinzadeh 2017) to obtain the difference image and to correspond to the statistics image (score image).

4.2.4. Transient Search

A vast majority of GIT observations are performed in “targeted mode,” typically having a single source of interest for photometry. However, for certain science goals like searching for poorly localized GRB afterglows and GW events counterpart searches, GIT undertakes “tiled mode” observations acquiring multiple contiguous images covering the sky region to which the transient has been coarsely localized. We run the image subtraction pipeline on these tiled mode observations. A subsequent pipeline with human-in-the-loop vetting is used for identifying transients in the subtracted images. We provide a very short overview here, and for details, refer the reader to H. Kumar et al. (2022, in preparation). Transient candidates are identified by locating the position of local peaks in the “score”

²⁴ <https://panstamps.readthedocs.io/>

image with s_{corr} value >5 . Among these, most of these detected candidates ($>99\%$) are spurious and filtered out by the candidates vetting pipeline. Finally, the remaining candidates are scanned by humans for verification. The interesting candidates thus obtained (if any) are further followed up to measure their evolution in time.

4.2.5. Processing Nonsidereal Data

The primary objective of nonsidereal observations with GIT is to report accurate astrometry and photometry of NEOs to MPC to reduce their orbital uncertainties. Images acquired in nonsidereal mode show all stars as streaks, with the target object ideally seen as a point source. We have developed another special pipeline to process such data: “Astrometry with Streaking Stars” (*Astreaks*; Sharma et al. 2021c). *Astreaks* identifies all the streaks in the image, generates an equivalent synthetic image with point sources, and solves it for astrometry using standard astrometry packages.²⁵ Astrometry obtained using this pipeline results in subarcsecond *Observed – Computed* residuals. Along with observations of Fast-Moving objects, we have also done follow-ups of multiple cometary outburst events. The aperture photometry of comets with centering is fully automated, given the aperture size. The GIT pipeline is also equipped with track-and-stack software designed to stack the data of moving targets, thus helping with better analysis of cometary features by improving the SNR. The detailed working of *Astreaks* is discussed in K. Sharma et al. (in prep).

4.3. Observation Reports and Data Archiving

GIT pipeline has been designed to produce standardized data products. The images obtained after the entire processing have standard headers and do not require any additional knowledge about GIT by users. Data processing is logged and reported on Slack in real time, which helps in debugging the unprecedented processing errors and tracking live-time processing progress. All raw and processed data are archived in network-attached storage (NAS) at IIT Bombay. Key data properties are also stored in a local queryable database which is populated right after the completion of processing of each image.

5. System Performance

5.1. On-sky Efficiency

GIT received its first light during the commissioning phase in 2018 June. At commissioning, the telescope and camera system was operated in manual mode, with remote and local operators sharing responsibilities. Since then, the system has been upgraded in a phased manner. In 2019 February, the system was upgraded into the semiautomated mode, where scripts managed the bulk of operations. However, a few tasks like dome operations, calibration frames acquisition, and system monitoring were handled by operators at the observatory. In 2021 September, GIT was upgraded to a fully automated mode. In the course of typical operations, the control software handles all responsibilities, including acquiring calibration images, calculating the observing schedule from the master target list, filter changes, target acquisition and tracking, operating the dome, filter wheel, camera, etc. For

absolute safety, the control software does not have the capability to operate the dome or telescope shutters: these are the only operations that require the physical presence of the observing assistant at the start and end of the observing program. The control software monitors various diagnostic parameters and is capable of first-order debugging. If the system encounters any problems which it cannot fix, it alerts observers via messages or phone calls through the various bots (Section 3.4).

We quantify the telescope performance in two efficiency parameters. The first is the “on-sky efficiency”: the fraction of the night (defined by nautical twilight) that was spent acquiring target images. Thus, even necessary operations like readout and slew are considered extraneous in this definition. GIT currently operates with typical nightly efficiencies of $\gtrsim 80\%$. We also define an “effective efficiency,” where we include the readout time as part of the exposure. In this case, the “effective inefficiency” arises from weather, technical issues, or slews (which can be optimized to some extent). On good observing nights, effective efficiencies as high as 94% have been achieved (Figure 4). In contrast, the median effective efficiency in manual mode operations was around 30%. Part of this can be attributed to the upgrades and testing that were a key feature of manual operations. In semiautomated mode, median effective efficiency rose to $\sim 60\%$. The highest efficiencies in manual or semiautomated nights were attained during campaigns where we monitor a single target for most of the night. This drastically reduced the need for telescopes or dome slews or any human intervention in general. Overall, the best efficiencies are obtained in fully automated observations. Figure 4 shows the clear increase in telescope utilization efficiency from manual to semiautomated and finally to fully automated observations. The low-efficiency tails of the semi- and fully automated observations arise from partial nights lost to weather problems and to occasional technical issues.

5.2. Sensitivity

GIT has good sensitivity, with a typical depth of ~ 20.5 – 21 magnitudes in 10 minute g' and r' exposures. The typical full-width at half-maximum for point sources in GIT data is $\sim 3''$. Figure 5 shows the 5σ limiting magnitudes of GIT images for various filters for data obtained between 2021 July to December. The median limiting magnitude is 20.44 in g' and 20.49 r' bands for data obtained on ± 5 days of the new moon. u' and z' band images are typically shallower due to a combination of attenuation, reflectivity, camera sensitivity, and background. The faintest magnitude achieved with a 120 minute coadd in the r' band was ~ 22.9 . In all bands, data obtained within ± 5 days of the full moon are relatively shallower by up to two magnitudes due to the brighter sky background. Very shallow images in Figure 5(a), with a limiting magnitude around 16, are ones acquired under very poor observing conditions, like partial clouds.

5.3. Photometric Accuracy

GIT images are calibrated by cross-matching the stars from the same field against the Pan-STARRS Data Release 1 (DR1; Chambers et al. 2016) for the $g' r' i' z'$ bands, and the SDSS DR12 catalog (Alam et al. 2015) for u' data. To check the reliability of photometric calibration for $g' r' i' z'$ bands, we selected observations obtained on several dark nights (new

²⁵ Discussion of *Astreaks* implementation <https://sites.google.com/view/growthindia/results/astreaks>.

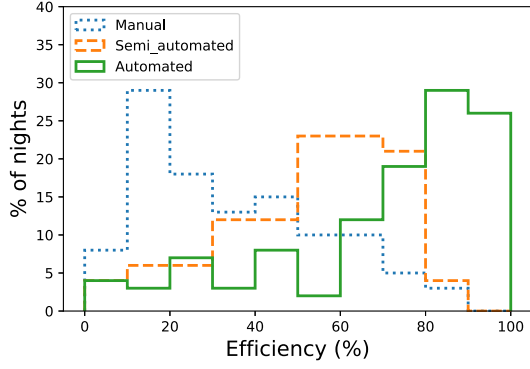


Figure 4. GROWTH-India Telescope efficiencies during each phase of operations. Three histograms show the efficiencies for manual mode (blue), semiautomated mode (orange), and automated mode (green). The system is currently running in automated mode with a typical efficiency of $\sim 80\%$, which is a noticeable improvement over the manual and semiautomated modes of observation. The low effacing tail in automated mode is due to unsuitable weather conditions and instrument failures.

moon ± 5 days), with airmass < 1.1 and exposure time 300 s. For the u' band, we used a stacked image of 600 s. In all bands, we limited the analysis to stars with a signal-to-noise ratio (S/N) > 10 . The photometric accuracy for various bands is plotted against the magnitudes of stars in Figure 5. Further, we derived photometric transformation equations between the GIT filter system and SDSS / Pan-STARRS filters. These transformation equations were obtained using a set of isolated stars in GIT images and reference catalogs. The transformation equations for Pan-STARRS and SDSS catalogs are listed below.

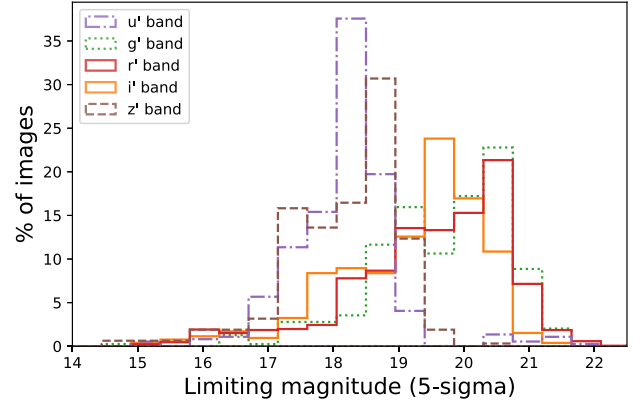
Transformations from Pan-STARRS to GIT magnitudes:

$$\begin{aligned} g'_{GIT} &= g_{PS} - 0.0051 * (g_{PS} - r_{PS}) + 0.0001, \sigma = 0.0067 \\ r'_{GIT} &= r_{PS} + 0.0016 * (g_{PS} - r_{PS}) - 0.0066, \sigma = 0.0165 \\ r'_{GIT} &= r_{PS} - 0.0085 * (i_{PS} - r_{PS}) - 0.0080, \sigma = 0.0178 \\ i'_{GIT} &= i_{PS} + 0.0091 * (i_{PS} - r_{PS}) + 0.0023, \sigma = 0.0133 \\ i'_{GIT} &= i_{PS} - 0.0158 * (i_{PS} - z_{PS}) - 0.0034, \sigma = 0.0252 \\ z'_{GIT} &= z_{PS} - 0.0408 * (i_{PS} - z_{PS}) - 0.0100, \sigma = 0.0159. \end{aligned}$$

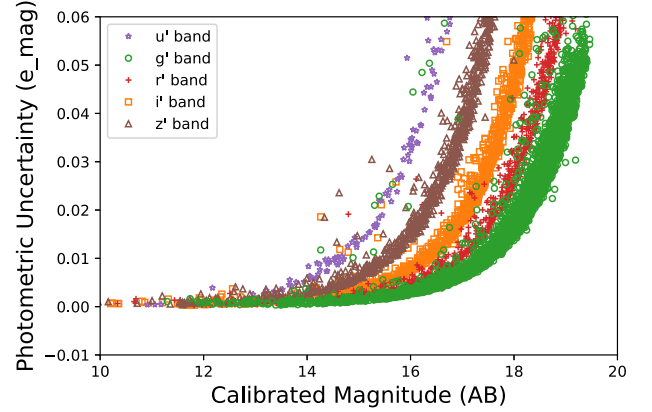
Transformations from SDSS to GIT magnitudes:

$$\begin{aligned} u'_{GIT} &= u_{SDSS} - 0.0168 * (g_{SDSS} - u_{SDSS}) + 0.1044, \\ &\sigma = 0.0565 \\ g'_{GIT} &= g_{SDSS} - 0.1486 * (g_{SDSS} - r_{SDSS}) + 0.0361, \\ &\sigma = 0.0378 \\ g'_{GIT} &= g_{SDSS} - 0.0719 * (u_{SDSS} - g_{SDSS}) + 0.0383, \\ &\sigma = 0.0389 \\ r'_{GIT} &= r_{SDSS} - 0.0077 * (g_{SDSS} - r_{SDSS}) + 0.0032, \\ &\sigma = 0.0104 \\ r'_{GIT} &= r_{SDSS} + 0.0021 * (i_{SDSS} - r_{SDSS}) - 0.0023, \\ &\sigma = 0.0071 \\ i'_{GIT} &= i_{SDSS} + 0.0091 * (i_{SDSS} - r_{SDSS}) + 0.0119, \\ &\sigma = 0.0194 \\ i'_{GIT} &= i_{SDSS} - 0.0132 * (i_{SDSS} - z_{SDSS}) - 0.0030, \\ &\sigma = 0.0224 \\ z'_{GIT} &= z_{SDSS} - 0.0251 * (i_{SDSS} - z_{SDSS}) + 0.0167, \\ &\sigma = 0.0165. \end{aligned}$$

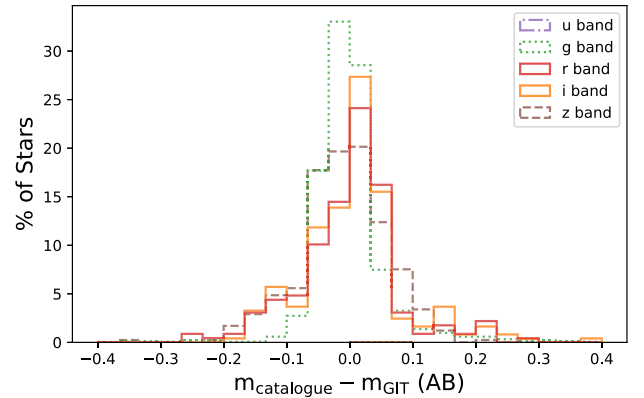
The higher color term for the g' transformation is consistent with the Pan-STARRS—SDSS hypercalibration (Finkbeiner et al. 2016).



(a)



(b)



(c)

Figure 5. (a) Limiting magnitude variation of GIT-Andor camera in SDSS u' g' r' i' z' bands for 300 s exposures. The g' and r' band images are deeper as compared to other bands due to low extinction and have a typical depth of 20.5 mag for 300 s exposure. (b) Photometric uncertainty for sources in various bands, as a function of source magnitude. (c) Photometric accuracy of GIT pipeline, measured as the difference between GIT and catalog magnitudes for all sources discussed in Section 5.3.

6. Science Results

The primary science goals for GIT are 1) The study of fast transients like gamma-ray bursts (GRBs) afterglows, electromagnetic counterparts to gravitational wave sources, fast radio bursts, fast blue optical transients, etc.; 2) follow-up of supernovae (SN) and novae from very early to late phases;

and 3) the study and characterization of solar system objects like near-Earth asteroids, active asteroids, comets, etc. In addition, the fourth goal of GIT is education—through courses, workshops, student training, etc. The last few years have been very productive for GIT in terms of scientific outcomes, aided by its robotic capabilities. Since commissioning, GIT has followed up a good number of SN, novae, GRB afterglows, EMGW candidates from GW merger events, near-Earth objects, and comets. Further, we performed the transient search observation for suitable events like Fermi GRBs with small localization uncertainty, GW event tiled follow-up, etc. The results from these observations are summarized in Section 6.1.

6.1. Afterglows of Gamma-Ray Bursts

GRBs have been the subject of great interest in the last two decades in astronomy. The afterglows of GRB arise due to the interaction of the jet with the surrounding medium at longer wavelengths than γ -rays. GRB optical afterglows are fast transients evolving on timescales of hours to days (Piran & Granot 2001). GIT’s autonomous operations and fast response time make these events a compelling science case for GIT. Since the first follow-up of such events in 2018 December (Srivastava et al. 2018), GIT has followed up on >70 GRB events with 20 detections and put constraints on optical brightness of >50 events. Figure 6 shows the comparison of GRB afterglow detections followed up by GIT to the Swift GRB optical afterglow population (Kann et al. 2011). We see that GIT has obtained dense sampling of several GRBs (see for instance Kumar et al. 2022) and that the afterglow candidates studied by GIT show similar fading characteristics as the broader sample of Swift GRBs.

Most of the GRB afterglows (>75%) were followed up within the first night from the trigger with a median response time of 0.55 days (including waiting for sunset). Our fastest turnaround time was 17 mins for GRB 210722A. Further, the independent discovery of the afterglow within the first hour of image acquisition for the GRB 200524A was one of the key highlights of the GRB follow-up effort. We did detailed follow-ups and analyses for a few other GRBs, including GRB 190114C, GRB 190530A, and GRB 210204A. The popular GRB 190114C detected at sub-TeV energies by MAGIC Telescope (Mirzoyan et al. 2019), was extensively followed up with GIT, and results were published in Misra et al. (2021). Results from the analysis of GRB 190530A were recently published in Gupta et al. (2022) where we probed into the emission mechanisms of this GRB. Another interesting GRB 210204A which showed deviations from typical synchrotron-driven afterglow emission at late times was followed up by GIT in coordination with other Indian facilities like HCT, DOT, and DFOT. A detailed study of this GRB was published in Kumar et al. (2022).

6.2. Supernovae

GIT has followed up on over 30 SNe of all types based on their visibility. GIT can be triggered immediately after discovery and has the capability to follow up to very late phases (>300 days). Very well-sampled light curves have been obtained for key targets. In Figure 7 we show r' -band light curves of a sample of core-collapse and thermonuclear SNe. GIT has often followed up on peculiar events, which can yield high scientific returns. For instance, SN 2018hna—an

SN 1987A-like explosion with shock breakout and a blue supergiant progenitor—has been studied in detail by Singh et al. (2019; Figure 7, left). A type Iax event, SN 2020sck, has been studied in Dutta et al. (2022). One-dimensional radiative transfer modeling of SN 2020sck (Figure 7, right) has shown the explosion to be a pure deflagration in a carbon–oxygen white dwarf.

In the left panel of Figure 7, we show GIT data with solid symbols, complemented with publicly available data in open symbols. For the type-II event SN 2021gmj, GIT data covered a crucial decline phase. The Ic event SN 2021mxx was covered through its peak, while SN 2021do was observed from the peak onwards. SN 2019vxx and SN 2019tua have been followed up mostly in the late phases. To understand the types of these events, we compare the early phase light curve of SN 2019tua with a type IIb event SN 1996cb (Qiu et al. 1999). Similarly, for SN 2019vxx, we compare it with type IIc event SN 2005ip (Stritzinger et al. 2012). GIT has complemented surveys like the Zwicky Transient Facility (ZTF; Bellm et al. 2019) in some phases of evolution of a few objects and can be instrumental in following up on crucial phases of transient evolution. In the right panel of Figure 7, we show GIT r -band light curves for four thermonuclear supernovae. A paper combining SN 2021wuf and SN 2019np is under preparation.

6.3. Novae

GIT has observed several novae, both galactic and extragalactic. We have monitored the outbursts of the remarkable recurrent nova in M31—M31N2008-12a—in 2018 (Srivastava et al. 2018), 2020, and 2021 (Basu et al. 2021). We have monitored the 2021 outburst of the Galactic recurrent nova RS Ophiuchi, as well as several classical novae, including V1674 Her, AT 2021ypn, and AT 2022uz (or M31N2022-01a). Monitoring novae in M31 has even led to a serendipitous observation of the classical nova, AT2022cpe, as early as an hour from the time of discovery (Basu et al. 2022).

6.4. Electromagnetic Counterparts of Gravitational Wave (EMGW) Events

GIT extensively followed up on EMGW events during the third observation run (O3) Ligo-Virgo Collaboration (LVC), which began in 2019 April (Abbott et al. 2021). The first phase of O3 (aka O3a), which lasted until the end of 2019 September, resulted in the detection of six binary neutron star (BNS) candidates and nine black hole—Neutron star (BHNS) merger candidates²⁶(Abbott et al. 2021). Among these, six events: GW190425/S190425z (second BNS merger event), GW190426_152155/S190426c, GW190814/S190814bv, S190901ap, S190910d, S190910h were followed by GIT. For all but the S190426c event, GIT primarily followed up on interesting candidates at the early times of their evolution. The photometric follow-up played an important role in eliminating the noninteresting candidates in search of counterparts of GW events (Kasliwal et al. 2020). Preliminary results of the follow-up were published in the form of GCN circulars (Kumar et al. 2019a, 2019b; Waratkar et al. 2019a, 2019b; Bhalerao et al. 2019a, 2019b), and detailed analyses were undertaken in collaboration with GROWTH partners (Kasliwal et al. 2020; Coughlin et al. 2019). For the “S190426c” event, we worked in

²⁶ <https://gracedb.ligo.org/latest/>

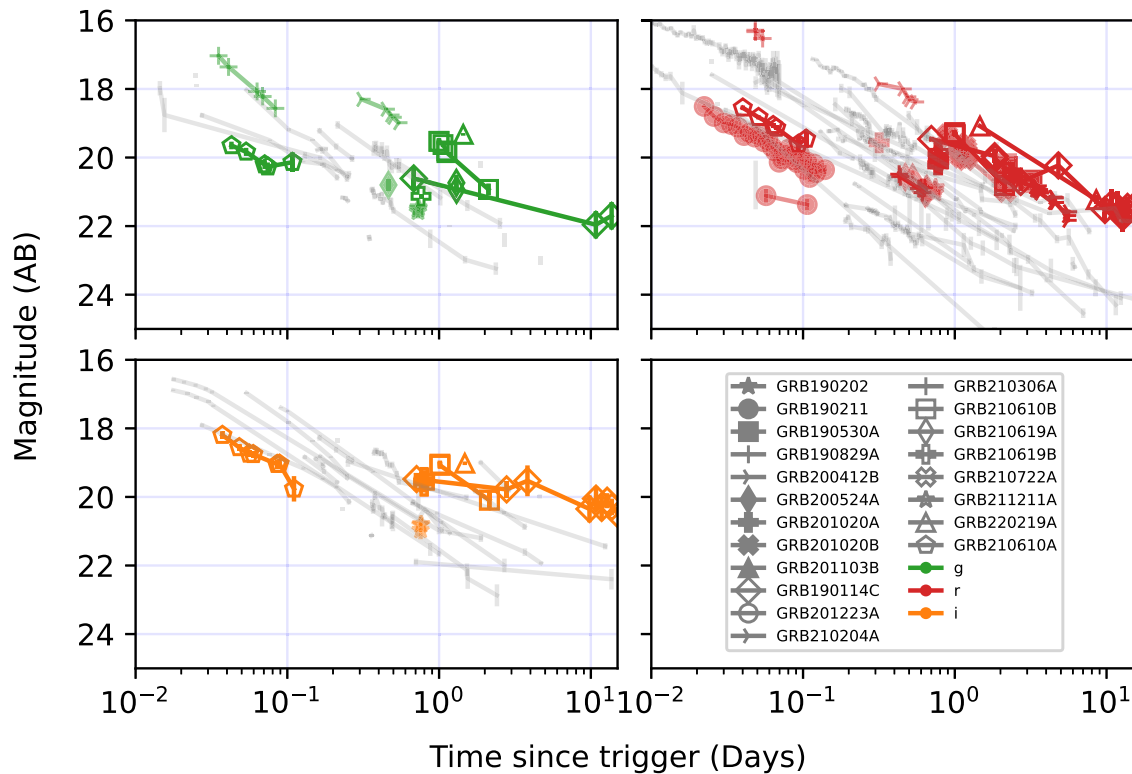


Figure 6. Light curves of GRB optical afterglow detections by GIT. The light curves of these afterglows in g' (top left panel), r' (top right panel), and i' (bottom left panel) bands have been plotted against the Swift GRB afterglow population taken from Kann et al. (2011). These afterglows span over the full range of Swift GRB afterglow population.

close collaboration with Zwicky Transient Facility (Bellm 2014 ZTF) and Dark Energy Camera (Flaugher et al. 2015 DECam) on Blanco Telescope to tile up a significant sky area (22.1 deg^2 area containing 17.5% localization probability) multiple times during the span of ~ 10 days. No viable candidate counterpart was detected in GIT follow-up observations. However, the upper limits obtained from follow-up observations helped put stringent constraints on ejecta masses from putative KNe (Kumar et al., 2022, in preparation).

6.5. Solar System Objects

GIT has an active follow-up observation program for near-Earth objects to refine their orbital parameters. To date, GIT has observed over one hundred NEOs with absolute magnitude up to $H \leq 27.7$ (see Figure 8).²⁷ Due to the high proper motion ($3.6\text{--}120''/\text{min}$), all the NEOs were observed with nonsidereal tracking.

GIT has been used to study seven periodic and sixteen nonperiodic comets. We have reported the cometary activity of four nonperiodic comets: C/2021 A6 (Bulger et al. 2020), C/2021 C1 (Rankin et al. 2020), C/2021 C3 (Pruyne et al. 2021), Comet C/2021 E3 (Bolin et al. 2021). In addition to the expected variation in brightness with the geocentric and heliocentric distances, a few comets showed outbursts, i.e., a short-term flare-up in luminosity (Hughes 1975). We undertook photometric follow-up of several cometary outbursts discovered by ZTF for confirmation of the event and further follow-up, including Comet 29P/Schwassmann-Wachmann 1 (Sharma et al. 2021b, 2021d; Kelley et al. 2021d), Comet C/2020 R4 (Kelley et al. 2021a),

Comet 22P/Kopff (Kelley et al. 2021b, 2021c), 67P/Churyumov-Gerasimenko (Kelley et al. 2021e; Sharma et al. 2021a).

Active asteroid (6478) Gault (originally designated as 1998 JC₁) is dynamically a main-belt asteroid with a Tisserand parameter with respect to Jupiter (T_J) = 3.46 (Ye et al. 2019). In 2020 June, we participated in coordinated observations with the GROWTH network to constrain its rotation period and understand its activity mechanism. With the help of coordinated observations, we measured a rotation period of ~ 2.5 hr (Purdum et al. 2021), which is the critical rotation period of a body of the size of Gault. It was concluded that the activity of Gault was due to surface mass shedding from its fast rotation spun up by the Yarkovsky–O’Keefe–Radzievskii–Paddack (YORP) effect (Bottke et al. 2006; Kleyna et al. 2019).

6.6. Fast Transients

A key component of GIT science involves the follow-up of rare, fast transients. One such event was AT2020xnd/ZTF20acimgel (the “Camel”), which evolved very fast, similar to the AT2018cow (the “cow”) event (Perley et al. 2019). The candidate maintained a high photospheric temperature even at a later stage of its evolution and with the absence of a second radioactive peak (Perley et al. 2021). We performed late-time deep follow-up in coordination with ZTF and Liverpool optical telescope (LT). A detailed analysis of this event was published by Perley et al. (2021). GIT followed up another interesting event AT2019pim/ZTF19abvizsw (Ho et al. 2020) in 2019 October. The candidate showed properties similar to an afterglow of a GRB. However, no GRB was detected for this event by high-energy monitors. The study of this orphan afterglow candidate is in progress and will soon be published in D. Perley et al. (2022, in preparation).

²⁷ Full list at <https://sites.google.com/view/growthindia/results/asteroids>.

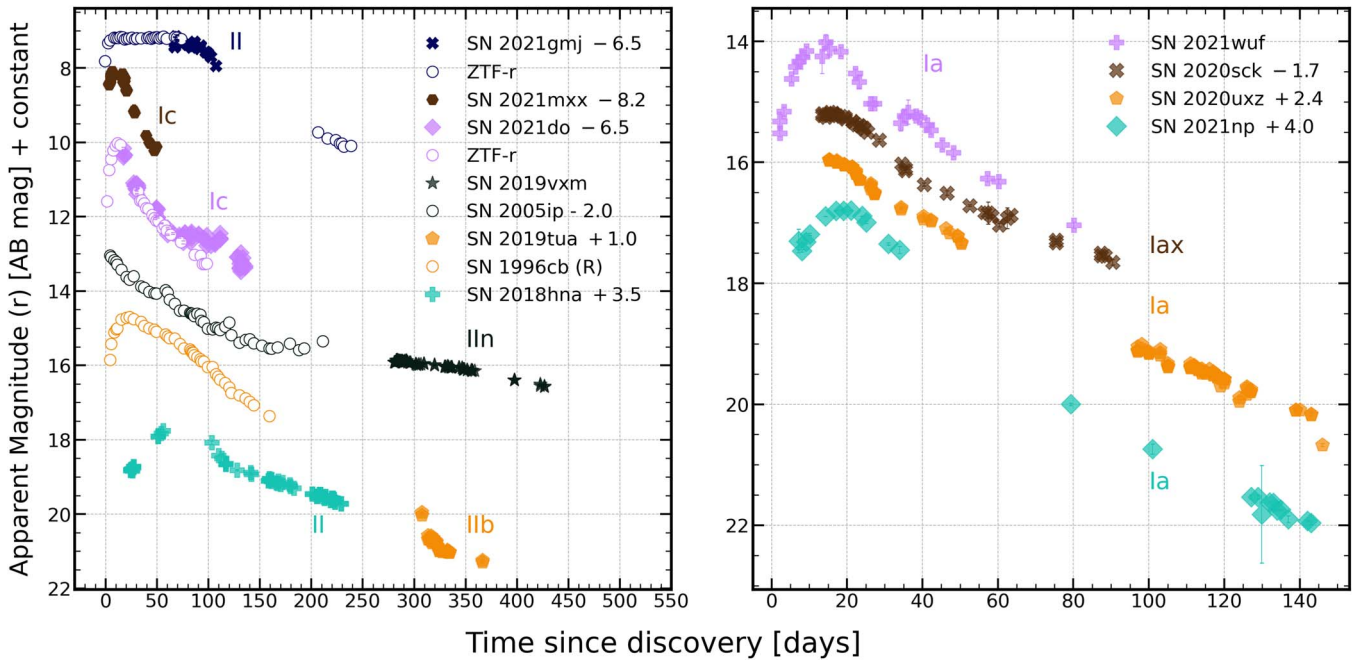


Figure 7. *r*-band light curves of a sample of supernovae observed with the GIT. The left panel shows the core-collapse objects, while the right panel shows the thermonuclear SNe. For SN 2019v_{xm} and SN 2019t_{ua}, GIT has missed the peak, and we show the early light curves of SN 1996cb (Qiu et al. 1999) and SN 2005ip (Stritzinger et al. 2012) to understand their possible type. GIT has complemented Zwicky Transient Facility (ZTF) surveys in some phases. For some SNe like SN 2021do and SN 2021gmj, we show the light curves in the *ZTF* - *r* band (Bellm et al. 2019).

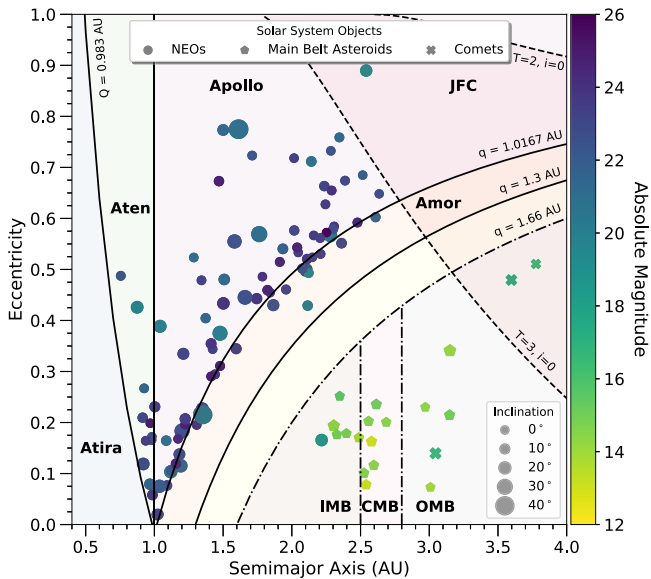


Figure 8. An (*a*, *e*, *i*) orbital distribution of all solar system objects observed with GIT. The region between perihelion $q = 1.3$ au and aphelion $Q = 0.983$ au demarcates the NEO regime. The orbital parameters of periodic comets with $a > 4$ au and nonperiodic comets are omitted here.

7. Summary

GROWTH-India Telescope is India’s first robotic telescope, located in Hanle. The telescope has been dedicated to time-domain astronomy since its commissioning in the summer of 2018. After starting its operation in manual mode for a few months, the system was upgraded in a phased manner to semiautomated mode and finally to an automated mode in 2021 September. These upgrades significantly increased the telescope’s “on-sky efficiency” to $>85\%$. The automated bots

handle monitoring of the system in real time and inform the core team of live-time observing updates and errors in case of automatic debug failure.

GIT has contributed to time-domain astronomy in the last few years by follow-up of EMGW events, GRBs, SNe, novae, and NEOs. More than 30 core-collapse and thermonuclear SNe have been followed up in the last 3 yr of observations. We have detected 20 GRB optical afterglows and provided useful constraints on the optical brightness of >50 GRB afterglows. We have performed an extensive follow-up of GW events from the O3 run of the advanced gravitational wave detector network, where we chose interesting candidates for follow-up and helped rule them out based on their evolution. During this run, we undertook an extensive transient search operation for S190426c that covered $>17.5\%$ of the total localization probability, which eventually constrained the mass ejection models for KNe. Follow-up of NEOs is a regular objective for GIT, where we have observed more than a hundred near-Earth objects and discovered/codiscovered four comet outbursts.

In addition to science, GIT has also been used for education—an important goal of the GROWTH network. The first international GROWTH school was conducted in India, including a live remote observing session at GIT.²⁸ The telescope contributes greatly to student training via courses, research projects, as well as undergraduate and graduate theses.

GIT’s automated operations and remarkable observing efficiency give it a unique place in Indian astronomy. In the near future, we are exploring various upgrades to operations, data processing, and hardware to further enhance the observatory’s performance. Equipped with these, GIT will continue to play an important role in time-domain astrophysics.

²⁸ <https://www.growth.caltech.edu/growth-winter-school-2018.html>

The GROWTH-India Telescope (GIT) is a 70 cm telescope with a 0.7 degree field of view, set up by the Indian Institute of Astrophysics and the Indian Institute of Technology Bombay with support from the Indo-US Science and Technology Forum (IUSSTF) and the Science and Engineering Research Board (SERB) of the Department of Science and Technology (DST), Government of India. It is located at the Indian Astronomical Observatory (Hanle), operated by the Indian Institute of Astrophysics (IIA). We acknowledge funding by the IITB alumni batch of 1994, which partially supports operations of the telescope. Telescope technical details are available at.²⁹

Harsh Kumar thanks the LSSTC Data Science Fellowship Program, which is funded by LSSTC, NSF Cybertraining Grant #1829740, the Brinson Foundation, and the Moore Foundation; his participation in the program has benefited this work.

This research has made use of the NASA/IPAC Extragalactic Database (NED), which is funded by the National Aeronautics and Space Administration and operated by the California Institute of Technology. This research has made use of NASA's Astrophysics Data System. This research has made use of data and/or services provided by the International Astronomical Union's Minor Planet Center. This research has made use of the VizieR catalog access tool, CDS, Strasbourg, France (DOI:10.26093/cds/vizieR). The original description of the VizieR service was published in 2000, A&AS 143, 23. This research made use of Astropy,³⁰ a community-developed core Python package for Astronomy (Astropy Collaboration et al. 2013, 2018).

Software: Astropy (Astropy Collaboration et al. 2013, 2018), Numpy (van der Walt et al. 2011), Matplotlib (Hunter 2007), Astro-SCRAPPY (McCully & Tewes 2019), Flask (Grinberg 2018), SExtractor (Bertin & Arnouts 1996), PSFEX (Bertin 2011), SWarp (Bertin et al. 2002), pyzogy (Guevel & Hosseinizadeh 2017), astrometry.net (Lang et al. 2010).

ORCID iDs

Harsh Kumar  <https://orcid.org/0000-0003-0871-4641>
 Varun Bhalerao  <https://orcid.org/0000-0002-6112-7609>
 G. C. Anupama  <https://orcid.org/0000-0003-3533-7183>
 Sudhanshu Barway  <https://orcid.org/0000-0002-3927-5402>
 Jadhajet Basu  <https://orcid.org/0000-0001-7570-545X>
 Kunal Deshmukh  <https://orcid.org/0000-0001-5253-3480>
 Kishalay De  <https://orcid.org/0000-0002-8989-0542>
 Anirban Dutta  <https://orcid.org/0000-0002-7708-3831>
 Christoffer Fremling  <https://orcid.org/0000-0002-4223-103X>
 Hrishikesh Iyer  <https://orcid.org/0000-0002-2395-8727>
 Adeem Jassani  <https://orcid.org/0000-0003-2191-4541>
 Simran Joharle  <https://orcid.org/0000-0002-8875-6413>
 Viraj Karambelkar  <https://orcid.org/0000-0003-3758-159X>
 Sumeet Kulkarni  <https://orcid.org/0000-0001-8057-0203>
 Sujay Mate  <https://orcid.org/0000-0001-5536-4635>
 DVS Phanindra  <https://orcid.org/0000-0002-1762-0834>
 Subham Samantary  <https://orcid.org/0000-0003-2167-9764>
 Kritti Sharma  <https://orcid.org/0000-0002-4477-3625>
 Yashvi Sharma  <https://orcid.org/0000-0003-4531-1745>
 Avinash Singh  <https://orcid.org/0000-0003-2091-622X>

Shubham Srivastava  <https://orcid.org/0000-0003-4524-6883>

Vishwajeet Swain  <https://orcid.org/0000-0002-7942-8477>

Gaurav Waratkar  <https://orcid.org/0000-0003-3630-9440>

Padma Dorjay  <https://orcid.org/0000-0001-5690-2212>

Tarun Kumar Sharma  <https://orcid.org/0000-0002-2966-2951>

Tsewang Stanzin  <https://orcid.org/0000-0002-1469-3958>

References

- Abbott, R., Abbott, T. D., Abraham, S., et al. 2021, *PhRvX*, **11**, 021053
- Alam, S., Albareti, F. D., Allende Prieto, C., et al. 2015, *ApJS*, **219**, 12
- Antier, S., Agayeva, S., Aivazyán, V., et al. 2020, *MNRAS*, **492**, 3904
- Astropy Collaboration, Robitaille, T. P., Tollerud, E. J., et al. 2013, *A&A*, **558**, A33
- Astropy Collaboration, Price-Whelan, A. M., Sipőcz, B. M., et al. 2018, *AJ*, **156**, 123
- Barthelmy, S. D., Cline, T. L., Butterworth, P., et al. 2000, in *AIP Conf. Ser.* 526, *Gamma-ray Bursts*, ed. R. M. Kippen, R. S. Mallozzi, & G. J. Fishman (Melville, NY: AIP), 731
- Basu, J., Kumar, H., Anupama, G. C., et al. 2021, *ATel*, **15038**, 1
- Basu, J., Kumar, H., Anupama, G. C., et al. 2022, *ATel*, **15250**, 1
- Bellm, E. 2014, in *The Third Hot-wiring the Transient Universe Workshop (HTU-III)*, ed. P. R. Wozniak et al. (Menlo Park, CA: SLAC), 27
- Bellm, E. C., Kulkarni, S. R., Graham, M. J., et al. 2019, *PASP*, **131**, 018002
- Bertin, E. 2011, in *ASP Conf. Ser.* 442, *Astronomical Data Analysis Software and Systems XX*, ed. I. N. Evans et al. (San Francisco, CA: ASP), 435
- Bertin, E., & Arnouts, S. 1996, *A&AS*, **117**, 393
- Bertin, E., Mellier, Y., Radovich, M., et al. 2002, in *ASP Conf. Ser.*, 281, *Astronomical Data Analysis Software and Systems XI*, ed. D. A. Bohlender, D. Durand, & T. H. Handley (San Francisco, CA: ASP), 228
- Bhalerao, V., Kumar, H., Karambelkar, V., et al. 2019a, *GCN*, 24258, 1
- Bhalerao, V., Kumar, H., Karambelkar, V., et al. 2019b, *GCN*, 24201, 1
- Bolin, B. T., ZTF Collaboration, Ip, W. H., Lin, Z. Y., & Masci, F. J. 2021, *Minor Planet Electronic Circulars*, MPEC 2021-J71 : COMET C/2021 E3 (ZTF), <https://cgi.minorplanetcenter.net/mpec/K21/K21J71.html>
- Botke, W. F., Jr, Vokrouhlický, D., Rubincam, D. P., & Nesvorný, D. 2006, *Annu. Rev. Earth Planet. Sci.*, **34**, 157
- Brown, A. G. A., Vallenari, A., Prusti, T., et al. 2018, *A&A*, **616**, A1
- Brown, T. M., Baliber, N., Bianco, F. B., et al. 2013, *PASP*, **125**, 1031
- Bulger, J., Lowe, T., Schultz, A., et al. 2020, *Minor Planet Electronic Circulars*, MPEC 2021-A210 : COMET C/2021 A6 (PANSTARRS), <https://www.minorplanetcenter.org/mpec/K21/K21A10.html>
- Chambers, K. C., Magnier, E. A., Metcalfe, N., et al. 2016, arXiv:1612.05560
- Coughlin, M. W., Ahumada, T., Anand, S., et al. 2019, *ApJL*, **885**, L19
- Cowsik, R., Srinivasan, R., & Prabhu, T. 2002, in *ASP Conf. Ser.* 266, *Astronomical Site Evaluation in the Visible and Radio Range*, ed. J. Vernin, Z. Benkhaldoun, & C. Muñoz-Tuñón (San Francisco, CA: ASP), 424
- de Zeeuw, P. T., & Molster, F. J. 2007, *A Science Vision for European Astronomy* (Milan: Astronet), https://www.eso.org/public/archives/books/pdfsm/book_0028.pdf
- Dhillon, V. S., Marsh, T. R., Stevenson, M. J., et al. 2007, *MNRAS*, **378**, 825
- Dhillon, V. S., Marsh, T. R., Bezawada, N., et al. 2016, *Proc. SPIE*, **9908**, 99080Y
- Dutta, A., Sahu, D. K., Anupama, G. C., et al. 2022, *ApJ*, **925**, 217
- Finkbeiner, D. P., Schlafly, E. F., Schlegel, D. J., et al. 2016, *ApJ*, **822**, 66
- Flaugher, B., Diehl, H. T., Honscheid, K., et al. 2015, *AJ*, **150**, 150
- Graham, M. J., Djorgovski, S. G., Stern, D., et al. 2015, *MNRAS*, **453**, 1562
- Grinberg, M. 2018, *Flask Web Development: Developing Web Applications with Python* (2nd edn.; Sebastopol, CA: O'Reilly Media)
- Grindlay, J., Tang, S., Simcoe, R., et al. 2009, in *ASP Conf. Ser.* 410, *Preserving Astronomy's Photographic Legacy: Current State and the Future of North American Astronomical Plates*, ed. W. Osborn & L. Robbins (San Francisco, CA: ASP), 101
- Guevel, D., & Hosseinizadeh, G. 2017, *Dguelv/Pyzogy: Initial Release*, v0.0.1, Zenodo, doi:10.5281/zenodo.1043973
- Gupta, R., Gupta, S., Chattopadhyay, T., et al. 2022, *MNRAS*, **511**, 1694
- Ho, A. Y. Q., Perley, D. A., Beniamini, P., et al. 2020, *ApJ*, **905**, 98
- Hughes, D. W. 1975, *QJRAS*, **16**, 410
- Hunter, J. D. 2007, *CSE*, **9**, 90
- Kann, D. A., Klose, S., Zhang, B., et al. 2011, *ApJ*, **734**, 96
- Kasliwal, M. M. 2011, PhD thesis, California Institute of Technology

²⁹ <https://sites.google.com/view/growthindia/>

³⁰ <http://www.astropy.org>

- Kasliwal, M. M., Cannella, C., Bagdasaryan, A., et al. 2019, *PASP*, **131**, 038003
- Kasliwal, M. M., Anand, S., Ahumada, T., et al. 2020, *ApJ*, **905**, 145
- Kelley, M. S. P., Lister, T., Sharma, K., et al. 2021a, *ATel*, **14618**, 1
- Kelley, M. S. P., Lister, T., Sharma, K., et al. 2021b, *ATel*, **14565**, 1
- Kelley, M. S. P., Sharma, K., Bhalerao, V., Anupama, G. C., & Barway, S. 2021c, *ATel*, **14628**, 1
- Kelley, M. S. P., Sharma, K., Kumar, H., et al. 2021d, *ATel*, **14543**, 1
- Kelley, M. S. P., Sharma, K., Swain, V., et al. 2021e, *ATel*, **15053**, 1
- Kleyna, J. T., Hainaut, O. R., Meech, K. J., et al. 2019, *ApJ*, **874**, L20
- Kumar, H., Karambelkar, V., Bhalerao, V., et al. 2019a, *GCN*, 24351, 1
- Kumar, H., Dutta, A., Waratkar, G., et al. 2019b, *GCN*, 25632, 1
- Kumar, H., Gupta, R., Saraogi, D., et al. 2022, *MNRAS*, **513**, 2777
- Lang, D., Hogg, D. W., Mierle, K., Blanton, M., & Roweis, S. 2010, *AJ*, **139**, 1782
- Lipunov, V., Kornilov, V., Gorbvskoy, E., et al. 2010, *AdAst*, 2010, 349171
- LSST Science Collaboration, Abell, P. A., Allison, J., et al. 2009, arXiv:0912.0201
- McCully, C., & Tewes, M. 2019, Astro-SCRAPPY: Speedy Cosmic Ray Annihilation Package in Python, Astrophysics Source Code Library, ascl:1907.03211
- Mirzoyan, R., Noda, K., Moretti, E., et al. 2019, *GCN*, 23701, 1
- Misra, K., Resmi, L., Kann, D. A., et al. 2021, *MNRAS*, **504**, 5685
- National Academies of Sciences, Engineering, and Medicine 2021, Pathways to Discovery in Astronomy and Astrophysics for the 2020s (Washington, DC: The National Academies Press)
- NRC Decadal Survey 2010, New Worlds, New Horizons in Astronomy and Astrophysics (National Academies Press) (Washington, DC: The National Academies Press)
- Perley, D. A., Mazzali, P. A., Yan, L., et al. 2019, *MNRAS*, **484**, 1031
- Perley, D. A., Ho, A. Y. Q., Yao, Y., et al. 2021, *MNRAS*, **508**, 5138
- Piran, T., & Granot, J. 2001, in *Gamma-ray Bursts in the Afterglow Era*, ed. E. Costa, F. Frontera, & J. Hjorth (Berlin: Springer), 300
- Pruyne, T. A., Kowalski, R. A., Rankin, D., et al. 2021, *Minor Planet Electronic Circulars*, MPEC 2021-D112 : COMET C/2021 C3 (Catalina), <https://www.minorplanetcenter.net/mpec/K21/K21DB2.html>
- Purdum, J. N., Lin, Z.-Y., Bolin, B. T., et al. 2021, *ApJL*, **911**, L35
- Qiu, Y., Li, W., Qiao, Q., & Hu, J. 1999, *AJ*, **117**, 736
- Rankin, D., Christensen, E. J., Farneth, A., et al. 2020, *Minor Planet Electronic Circulars*, MPEC 2021-D102 : COMET C/2021 C1 (Rankin)., <https://www.minorplanetcenter.net/mpec/K21/K21DA2.html>
- Sagar, R. 2017, *PINSA*, **87**, 1
- Sharma, K., Kelley, M. S. P., Joharle, S., et al. 2021a, *RNAAS*, **5**, 277
- Sharma, K., Kelley, M. S. P., Swain, V., et al. 2021b, *ATel*, **14898**, 1
- Sharma, K., Kumar, H., Bolin, B., et al. 2021c, *EPSC*, **1**, EPSC2021
- Sharma, K., Kelley, M. S. P., Lister, T., et al. 2021d, *ATel*, **14984**, 1
- Singh, A., Sahu, D. K., Anupama, G. C., et al. 2019, *ApJL*, **882**, L15
- Srinivasan, G., Chitre, S. M., Nityananda, R., & Tandon, S. N. 2004, *Astronomy and Astrophysics: A decadal vision document*, <https://www.ias.ac.in/public/Resource1161es/OtherPublications/Overview/astrophys.pdf>
- Srivastav, S., Pavana, M., Stanzin, U., et al. 2018, *ATel*, **12203**, 1
- Srivastava, S., Kumar, H., Otzer, S., et al. 2018, *GCN*, 23510, 1
- Stalin, C. S., Hegde, M., Sahu, D. K., et al. 2008, *BASI*, **36**, 111
- Stritzinger, M., Taddia, F., Fransson, C., et al. 2012, *ApJ*, **756**, 173
- van der Walt, S., Colbert, S. C., & Varoquaux, G. 2011, *CSE*, **13**, 22
- Waratkar, G., Kumar, H., Bhalerao, V., et al. 2019a, *GCN*, 24316, 1
- Waratkar, G., Kumar, H., Bhalerao, V., Stanzin, J., & Anupama, G. C. 2019b, *GCN*, 24304, 1
- Ye, Q., Kelley, M. S. P., Bodewits, D., et al. 2019, *ApJ*, **874**, L16
- Zackay, B., Ofek, E. O., & Gal-Yam, A. 2016, *ApJ*, **830**, 27